Biotechnology at Low Reynolds Numbers

James P. Brody, Paul Yager, Raymond E. Goldstein, and Robert H. Austin

Center for Bioengineering, University of Washington, Seattle, Washington 98195-2141, and Department of Physics, Princeton University, Princeton, New Jersey 08544 USA

ABSTRACT   The shrinking of liquid handling systems to the micron and submicron size range entails moving into the area of small Reynolds numbers. The fluid dynamics in this regime are very different from the macroscale. We present an intuitive explanation of how the different physics of small Reynolds numbers flow, along with microscopic sizes, can influence device design, and give examples from our own work using fluid flow in microfabricated devices designed for biological processing.

INTRODUCTION

It has recently become possible, using the power of microfabrication, to construct fluid systems with feature sizes as small as a few microns. There has been a surge of interest in the "lab-on-a-chip" concept, which involves the miniaturization of many chemical processes onto a single silicon chip (Ramsey et al., 1995). Because these systems allow one to manipulate single cells, and even single macromolecules, there is great interest in the biotechnology community in using microfluid systems for analytical tests. For example, in the polymerase chain reaction, amplification of DNA in a microenvironment is attractive both because the temperature can be rapidly cycled and because the sample volume is extremely small (Wilding et al., 1994; Northrup et al., 1995). Other examples of uses for micromachining in biology would be the construction of arrays for the filtration and fractionation of DNA and cells (Volkmuth and Austin, 1992; Brody et al., 1995), where the precise machinability of silicon and control over the size of the structures is very important. There have been a number of other microfabricated devices constructed for simple analytical tests (Ramsey et al., 1995). Many of these use electrokinetic forces to induce flow, and the physics of this is in some cases different from the pressure-driven flow discussed here. See Manz et al., 1993, for a detailed discussion of electrokinetically driven devices. We have chosen in this article to concentrate on hydrodynamic flow issues. There are four microfabricated devices used as examples in this paper: a percolating lattice through which DNA molecules move, a hydrodynamically focused fast mixing device to study protein folding reactions, a virtual valve used to direct flow at the intersection of multiple channels, and a diffusion-based extraction device.

As fluid transport systems get smaller and smaller, they inevitably move to the regime of viscous dominated flow, as the characteristic length scale of the flow shrinks with the

size of the device. There is a fundamental change in hydrodynamics that occurs here, which can act as a barrier to the operation of the device. This barrier occurs when the Reynolds number is of order unity. For practical purposes, with water as the working fluid, one enters the low Reynolds number regime when the channel size is smaller than about 100 μm with fluid velocities on the order of μm/s. The fluid dynamics at this size scale are somewhat different from what one finds in everyday experience. An informal, intuitive explanation of many of these effects is found in a classic paper (Purcell, 1977). At these scales, viscous forces dominate over inertial forces, turbulence is nonexistent, surface tension can be a powerful force, diffusion becomes the basic method for mixing, and evaporation acts quickly on exposed liquid surfaces. This paper outlines the laws that govern fluid phenomena at small scales, explores the effect of diffusion and surface tension on these fluid flows, and presents results from a few basic experiments.

MICROMACHINING AND FLOW VISUALIZATION

Micromachining involves the use of either energetic ion plasmas or wet chemical etches to selectively remove and undercut material from objects, typically silicon wafers with deposited or thermally grown surface layers. An extensive review of these techniques can be found in Peterson, 1982. Here, patterns are constructed on silicon wafers using photolithography, then etched using either chlorine-based reactive ion etching or anisotropic wet etches, and finally anodically bonded to Pyrex windows (Wallis and Pomerantz, 1969; Volkmuth, 1994; Brody et al., 1995). This process can be used to form arbitrary shapes of microfluid flow channels, as we show in Fig. 1. This complicated network of flow channels (a percolating lattice) can be created with ease using microfabrication. The algorithm used to construct pseudorandom structures begins with a square grid of points. For each line between two adjacent grid points a random number between 0 and 1 is chosen. If the number is larger than some predetermined limit, in this case 0.4, a line is drawn, otherwise the line is left blank. As long as the filling probability is kept less than the percolation limit, there exists a path through the structure. A standard process was used at the Cornell Nanofabrication Facility (CNF) in
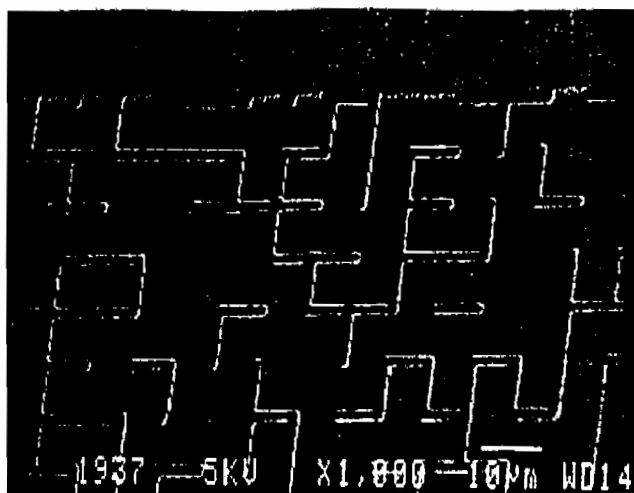
FIGURE 1 A scanning electron micrograph of a percolating lattice, in this case etched into a conducting doped poly-silicon layer. A piece of Pyrex glass was anodically bonded to the tops of these rectangular blocks to hermetically seal the flow chamber. (SEM by Rich Tiberio, NNF).

Ithaca, NY (Brody et al., 1995) and an alternative wet chemical process was used at the Washington Technology Center (Brody and Yager, 1996).

To provide a fluid entrance to the device, a small hole was carefully ground through a piece of Pyrex glass. The glass was then anodically bonded to the tops of the silicon blocks, and a glass tube was epoxied over the hole, as shown in Fig. 2. An alternative is to etch a hole completely through the silicon and make fluid connections on the back side of the device. The fluid flow was driven by a pressure gradient. Large pressure differences (greater than 5 psi) were set and controlled by using either a compressed gas source behind a liquid reservoir or a syringe with manually applied pressure. Smaller, easily controllable, pressure heads can be produced by a column of water.

Fluorescent microscopy is an ideal tool for flow visualization in microfluidic systems. Submicron diameter neutral buoyant spheres impregnated with fluorescent dyes are commercially available (Duke Scientific, Palo Alto, CA; Polysciences, Warrington, PA). We have used these spheres, DNA molecules, free fluorescent dye, and fluorescent-tagged protein to visualize both flow patterns and diffusion in microfabricated structures. In a typical experiment a 0.01% solution of 0.5-μm diameter fluorescing beads was used to visualize the flow. These beads were imaged either on a Nikon Optiphot compound microscope or on an inverted Zeiss microscope. Depending on the size of the signal, a Hamamatsu 2400 SIT camera, Dage silicon-intensified target (SIT) video-rate camera, or a GBC CCD (CCTV Video, Inc.) camera, in order of decreasing sensitivity and increasing frame rates, was used to image the objects. The video data were recorded on S-VHS video tape and analyzed later on a Silicon Graphics Indy computer and a Macintosh 636 Performa computer.
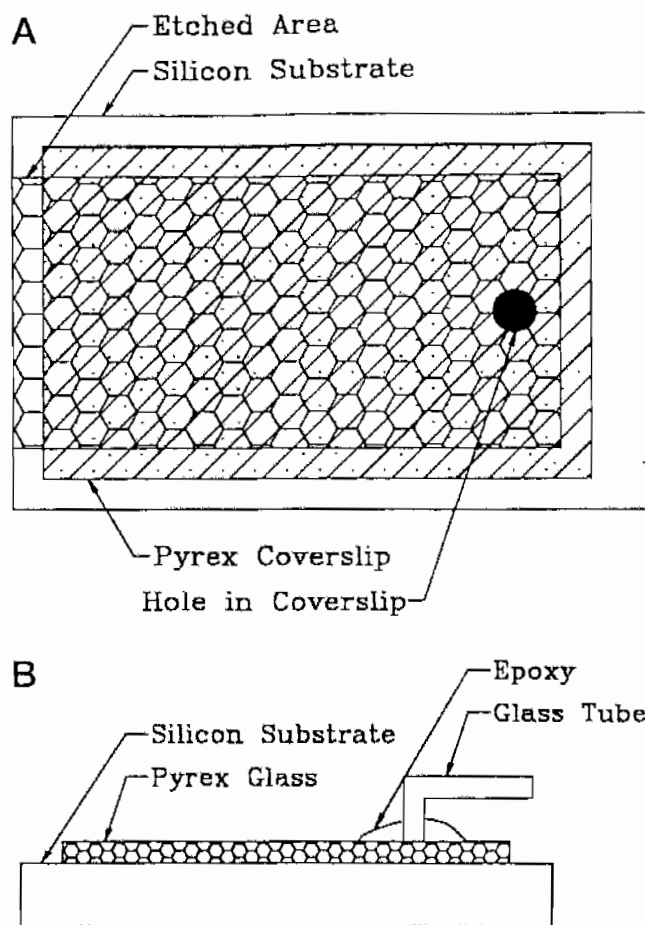

FIGURE 2 Top (a) and side (b) views of the experimental setup. The thickness of the materials is not drawn to scale.

FLUID DYNAMICS

The basic equation governing incompressible fluid dynamics is the Navier-Stokes equation,

$$\rho\left[\frac{\partial \mathbf{u}}{\partial t} + (\mathbf{u} \cdot \nabla)\mathbf{u}\right] = -\nabla P + \eta \nabla^2 \mathbf{u}. \qquad (1)$$

where $\mathbf{u}$ is the fluid velocity, P is the pressure, and η is the fluid viscosity. The Navier-Stokes equation is just Newton's law for a fluid, with forces per unit volume on the right-hand side due to a pressure gradient, $(-\nabla P)$, and viscosity, $(\eta \nabla^2 \mathbf{u})$. The left-hand side gives the mass per unit volume, ρ, times the acceleration of the fluid, expressed in terms of the convective derivative in a Eulerian representation. Additional body forces acting on the fluid add to the right-hand side (e.g., gravity as a term ρg).

The Reynolds number serves to measure the ratio of the inertial forces to the viscous forces. This ratio may be written as

$$Re = \rho \frac{u/t + u^2/l}{\eta u/l^2}, \qquad (2)$$

where u, l, ρ, and η are, respectively, a characteristic fluid speed, length scale (e.g., channel diameter over which changes in the fluid velocity occur), density, viscosity, and where t is a characteristic time of the flow over which the velocity *vector* of the fluid flow changes appreciably in amplitude or direction. Inasmuch as $t \times u \sim l$, equation 2 can be rewritten as:

$$Re = \frac{\rho u l}{\eta}. \qquad (3)$$

At low Reynolds numbers, the fluid dynamics are dominated by viscous drag rather than by inertia, and because of this, devices that rely on inertial effects for their operation will no longer work. This leads to a limit to the extent to which one can scale down a design that works at high Reynolds numbers. If, however, a device is designed properly, it can work *better* as it gets smaller. The approximations made in viewing the system as dominated by viscous forces will be valid as long as the Reynolds number is <1 and the time scale ("switching time"), τ_s, on which the pressure driving the flow varies is longer than the time $\rho l^2/\eta$. Note that the smaller the diameter of a fluid channel, the *faster* such changes can be made.

Flow patterns are usually classified into one of two kinds, turbulent and laminar flow. Laminar flow is smooth predictable flow, which always occurs at $Re \ll 1$, where any induced vortices die away. Turbulent flow, which can only occur at high Reynolds numbers (typically $Re > 10^3$), is a situation in which inertial forces are much larger than viscous forces. It is characterized by a rich and complicated flow structure of interacting vortices. By carefully avoiding any instabilities, however, laminar flow conditions have been observed at Re higher than 10^5. The region of Re from 10^2 to 10^4 is generally regarded as the transition region between laminar and turbulent flow inside a channel. There is *never any turbulence in low Reynolds number flow.*

For fluid flow through microstructures studied in this work, some typical values for flowing water are, $u = 1-100$ μm/s and $l = 10$ μm. (See Table 1 for the physical constants related to water.) This gives a typical $Re = 10^{-3}$ to 10^{-5}. At low Re, like these, the Navier-Stokes equation is particularly simple, as we can effectively ignore the left-hand side of Eq. 1, which gives the inertial terms. This transforms a nonlinear partial differential equation into a simple linear one. The fluid flow is determined entirely by the pressure

distribution, the incompressibility constraint $\nabla \times \mathbf{u} = 0$, and, of course, the boundary conditions ($\mathbf{u} = 0$ at the walls). This type of flow is known by various names: "Stokes Flow," "Creeping Flow," "Potential Flow," or most simply and clearly, "Low Reynolds Number Flow." The governing law is the Stokes equation:

$$\eta \nabla^2 \mathbf{u} = \nabla P, \qquad (4)$$

a well-studied differential equation in mathematical physics.

Unlike the Navier-Stokes equation (Eq. 1), eq. 4 contains no time derivatives. Because of this, under low-Reynolds-number conditions, *all motion is symmetric in time*. Thus, if the pressures or forces exerted on the fluid are reversed, the motion in the fluid is completely reversed (Purcell, 1977). At high Reynolds numbers, it is virtually impossible to move a fluid and then return it to its original state, but this is easily done at low Reynolds numbers.

An important consideration in the design of any microfabricated structure is the influence that the boundaries of a flow chamber have on the flow profile. Such effects determine the relationship between pressure gradients and volumetric flow rates, the uniformity of velocity profiles transverse to the mean flow direction, as well as aspects of advection-enhanced diffusion (that is, enhancement of mixing by shearing flow—Taylor diffusion). In this section we consider the two basic flow geometries, pipe and channel flow, and study the solutions to the Stokes equation for steady flow. The standard boundary conditions that we will assume throughout this text are "no-slip" boundary conditions, meaning that at the surface of an object there is no fluid flow. [These conditions are well established even at the submicron level (Bocquet and Barrat, 1993).] Using fluorescent beads as tracer particles in the flow, we present the results of a visualization of the boundary layers that form near walls in wide-aspect ratio channels due to the no-slip boundary conditions.

The most important physical situation encountered is flow down a channel, and surprising predictions for the flow profile are easy to obtain. For both pipe and channel flow, we consider a conduit of infinite extent in the z-direction, with a (fixed) pressure gradient:

$$\frac{\partial P}{\partial z} = -G, \qquad (5)$$

with $G > 0$. The velocity field is $\mathbf{u}(x, y) = u(x, y)\hat{e}_z$, and is automatically divergence-free for any scalar function $u(x, y)$.

In the case of pipe flow (cylindrical symmetry), the azimuthal symmetry yields

$$\frac{1}{r}\frac{\partial}{\partial r}\left(r\frac{\partial u}{\partial r}\right) = -\frac{G}{\eta}. \qquad (6)$$

with boundary condition $u(R) = 0$. This is solved by

$$u(r) = \frac{G}{4\eta}(R^2 - r^2). \qquad (7)$$

TABLE 1   Scaling behavior of parameters for a constant-time micro-fluid device

Volume	l^3
Reynolds number	l^2
Length	l^1
Applied pressure	l^1
Fluid velocity	l^{-1}
Pressure due to surface tension	l^{-1}
Evaporation rate	l^{-1}
Diffusion time	l^{-2}

This is the usual parabolic flow profile.

Next we consider flow in a channel of width w and height h, with the origin of coordinates on the centerline. Fig. 3 shows schematically the dimensions of the channel. The Stokes equation is

$$\left(\frac{\partial^2}{\partial x^2} + \frac{\partial^2}{\partial y^2}\right)u = -\frac{G}{\eta},\tag{8}$$

with boundary conditions $u(-w/2, y) = u(w/2, y) = u(x, -h/2) = u(x, h/2) = 0$. When the aspect ratio

$$\epsilon = \frac{h}{w}\tag{9}$$

tends to zero, we obtain the classic Hele-Shaw geometry, and expect the flow to be described by Darcy's law (Bensimon et al., 1986), with a parabolic flow profile in the y-direction between the walls.

However, typically ϵ is finite. Mindful of the no-slip boundary conditions on the top and bottom walls, we obtain the solution to finite ϵ as a Fourier series

$$u(x, y) = \sum_{l=0}^{\infty} A^{(l)}(x) \cos[(2l + 1)\pi y/h].\tag{10}$$

By direct substitution one finds that the coefficients $A^{(l)}$ satisfy the differential equations

$$\frac{\partial^2 A^{(l)}}{\partial x^2} - \frac{(2l + 1)^2 \pi^2}{h^2} A^{(l)} = -\frac{4G(-1)^l}{\eta\pi(2l + 1)}.\tag{11}$$

The particular solutions are just constants, while the general homogeneous solutions are of the form $\cosh[(2l + 1)\pi x/h]$. Enforcing the boundary conditions then leads to the final result

$$u(x, y) = \left(\frac{Gh^2}{8\mu}\right)\frac{32}{\pi^2} \sum_{l=0}^{\infty} \frac{(-1)^l}{(2l + 1)^3}$$

$$\times \left\{1 - \frac{\cosh[(2l + 1)\pi x/h]}{\cosh[(2l + 1)\pi w/2h]}\right\}\tag{12}$$

$$\cdot\cos[(2l + 1)\pi y/h]$$

A useful check on this result is the limit $h \to 0$ at fixed x (with $|x| < w/2$), in which one finds

$$\lim_{\epsilon \to 0} u(x, y) = \frac{G}{8\eta}(h^2 - 4y^2)\tag{13}$$

Thus at any fixed point x away from the walls the flow profile becomes the familiar parabolic one as the depth of the channel tends to zero. For finite ϵ, the averaged flow has a boundary-layer character, varying rapidly near the walls on a scale of order h, but approaching a very flat, low gradient profile in the center of the channel.

It is natural to define a y-averaged velocity

$$\bar{u}(x) = \frac{1}{h}\int_{-h/2}^{h/2} dy\, u(x, y),\tag{14}$$

which takes the simple form

$$\bar{u}(x) = \left(\frac{Gh^2}{12\eta}\right)\frac{96}{\pi^4} \sum_{l=0}^{\infty} \frac{1}{(2l + 1)^4}$$

$$\cdot\left[1 - \frac{\cosh((2l + 1)\pi x/h)}{\cosh((2l + 1)\pi w/2h)}\right].\tag{15}$$

It is easily verified that this averaged velocity tends to the Darcy law result $\bar{u} = Gh^2/12\eta$ as the aspect ratio tends to zero.

Fig. 4 shows the expected y-averaged velocity $\bar{u}(x)$ for flow in a rectangular channel as a function of ϵ. The velocity values have been normalized. Note that while along the narrow aspect of the channel the flow remains parabolic, for
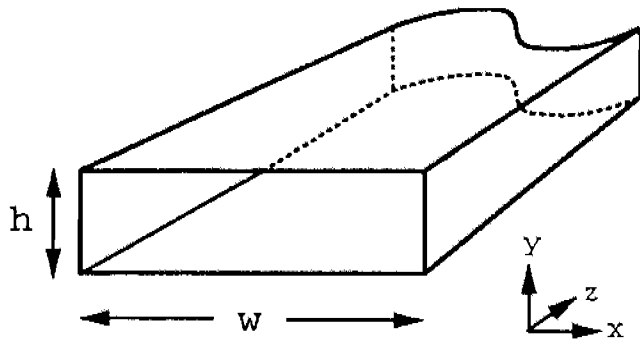
FIGURE 3   Geometry of channel flow. Quantities are defined in the text. The channel is assumed to be infinite in length.
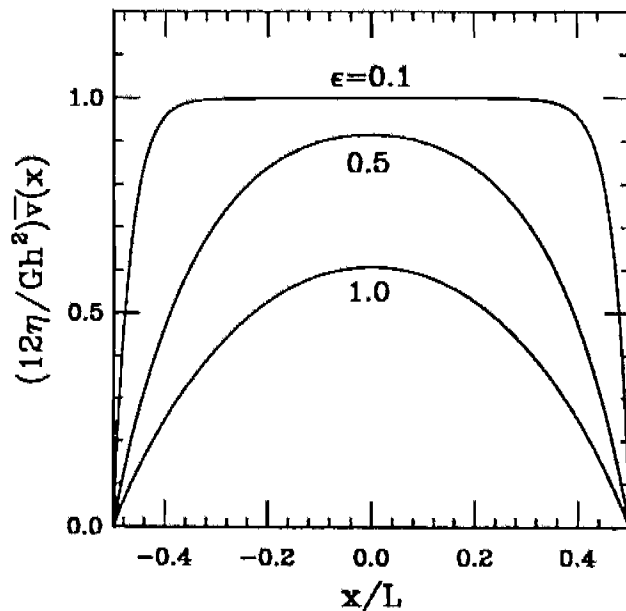
FIGURE 4   Maximum fluid velocity as a function of the transverse dimension across the channel x and the aspect ratio of the channel ϵ, as predicted by Eq. 15. The velocities have been normalized.

decreasing ϵ the average velocity as a function of x is increasingly plug-like. The distance over which the flow changes from the constant value to the stick boundary condition is approximately the narrow dimension h.

Written in terms of both the maximum velocity, u_{max}, and the volumetric flow rate, Q, Hele-Shaw flow and Poiseuille flow are governed by the relations

$$G = \frac{8\eta u_{max}}{h^2} = \frac{12\eta Q}{h^3 w}. \quad \text{(Hele-Shaw)} \qquad (16)$$

and

$$G = \frac{16\eta u_{max}}{d^2} = \frac{128\eta Q}{\pi d^4}, \quad \text{(Poiseuille)} \qquad (17)$$

where d is the diameter of the tube. The mean velocity is 2/3 of the maximum in Hele-Shaw flow, and 1/2 of the maximum in Poiseuille flow. Equation 17 is sketched graphically in Fig. 5, as it sets important constraints on the pressures needed to achieve given volumetric flow rates and velocities in microstructures. The maximum velocity for Hele-Shaw flow can also be read off of the figure by associating the diameter with the spacing between the plates, h, and doubling the associate velocity.

It is very important to point out that parabolic flow profiles pose serious problems for transport of solutes, because the effect of this gradient is to *spread out*, or dilute, a pulse of solute inserted into a solvent as a plug at some point in the flow (Taylor, 1953). Plug transport is the term used for the diffusive averaging of solute transport in which the averaged velocity of the transport of solute is constant across the face of the channel. Ideally, one would want plug transport profiles for many applications. However, although the local velocity of the fluid is zero at the walls and a maximum in the center, particles can move through a cylindrical tube with a plug profile. If the time, r^2/D, for the particles to diffuse across the radius r of the tube is less than r/u_{max} (where u_{max} is the maximum velocity), the particles will flow with effectively a plug profile at $u_{max}/2$. Thus, we have two regimes of flow,

$$D \gg r u_{max}, \quad \text{(plug transport)} \qquad (18)$$

and

$$D_{para} \ll r u_{max} \quad \text{(parabolic transport)}. \qquad (19)$$

In other words, if the solute molecules are small, such as the water solvent, and thus have a relatively large diffusion coefficient, they move with a plug profile. The above relations can be related to the Reynolds number, Eq. 3. For instance, typical small molecules in water ($D = 10^{-5}$ cm^2/s) move in a plug profile whenever $Re < 10^{-3}$.

The essential phenomenon in chemistry of mixing can also influence the pattern and flow of solvents in micron-size devices. Mixing consists of uniformly distributing all molecules in the solution throughout the vessel. It can occur essentially by two means: through fluid transport, which occurs at large geometries, or through diffusion, which dominates at micron scales. Each process has a characteristic time associated with it. The time it takes for a molecule to diffuse a distance D varies as the square of the distance, so that while relying on diffusion alone to mix things over a few centimeters is impractical, it is a quick and efficient process at the micron scale (Fig. 6).
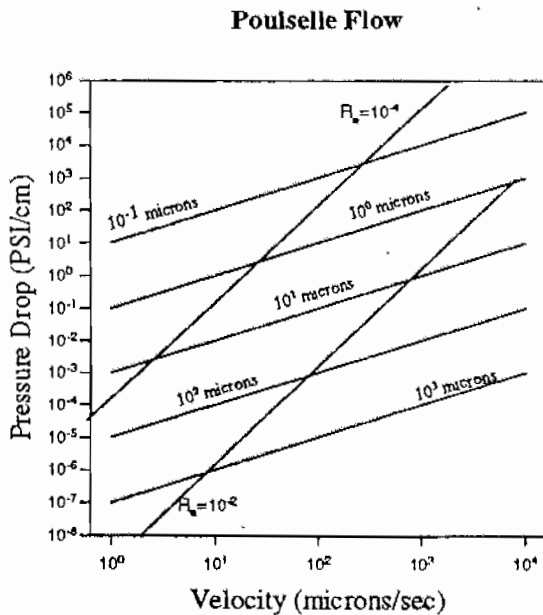

Poulselle Flow

FIGURE 5   Pressure gradient needed for a particular mean velocity of water flowing through tubes of different radii. Lines of constant Reynolds number are also shown.

Mixing Times

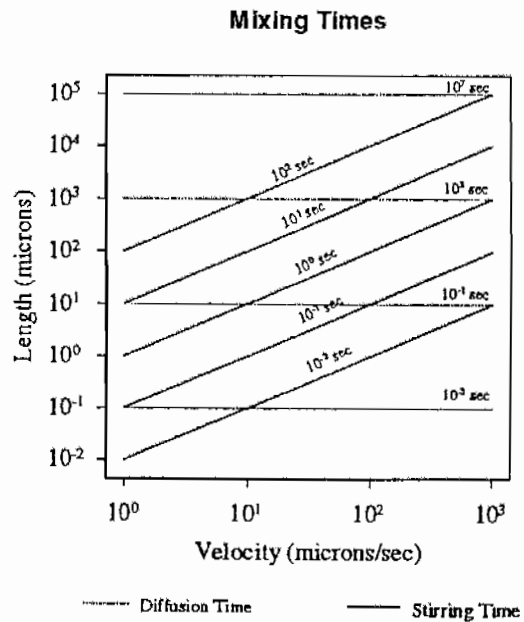------ Diffusion Time   —— Stirring Time

FIGURE 6   The characteristic time for mixing by stirring and diffusion. The time to diffuse is independent of the velocity, to first order. The velocity is the stirring velocity, for instance with a stir bar it would be ωr, the angular velocity times the length of the stir bar.

At some scale, all mixing is done by diffusion, but by stirring a binary mixture one can disperse the two fluids throughout the container so that the diffusion length for the system to become completely mixed is much smaller than it originally was. If we just ignore diffusion, the time required to mix two fluids together by stirring can be characterized by $t_s = l_s/v_s$, where l_s is the characteristic size and v_s is the characteristic stirring velocity (Purcell, 1977). At sizes above a few hundred microns, diffusion is so slow it can effectively be ignored. Inasmuch as at low Reynolds numbers any fluid velocity introduces shear, and shear will disperse the fluid, any stirring will help mixing. But there can be a huge difference between a good stirring strategy and a bad one. A good stirring strategy is one that is asymmetric in time (Purcell, 1977), for instance a stir bar spinning continuously in one direction. A bad stirring strategy is one that is symmetric in time. A piston moving in and out of the fluid is symmetric in time. This will not work well because after one cycle the fluid will return to exactly the original state (in the limit of $Re = 0$). In effect there has been no stirring at all.

To quantify the very efficient mixing by diffusion at small-size scales, recall that most small molecules in water have a diffusion coefficient of about $D = 10^{-5}$ cm²/s. The time to mix by diffusion is

$$t_D = \frac{l^2}{D} \quad (20)$$

where l is the largest size of the container. See Table 2 for the time required to diffuse a certain distance. Since the mixing time scales lineary with length scale, while the diffusion time is quadratic, we see that simply by reducing the length scales (and hence the Reynolds number), we go from the regime where the diffusion time is negligible compared with mixing and convection times to one where diffusion can be extremely important.

The diffusion coefficient for any particle,

$$D = \frac{kT}{6\pi\eta a}, \quad (21)$$

depends on the effective size of the particle a, the viscosity of the fluid the particle is in, η, and the absolute temperature, T. The linear size, a, of a molecule generally varies as the cube root of the molecular weight ($a \sim (MW)^{1/3}$), so the diffusion coefficient for a large protein is only about 10 times smaller than for a water molecule. For particles like cells (10 μm diameter) the diffusion constant could easily be 1000 times smaller than for a large protein. See Table 3 for a listing of characteristic times for various objects and length scales.

As an example of where these issues are important, consider microscale electrophoresis. The basic idea here is to shrink everything down to very small-length scales and volumes and use precisely designed confining lattices to optimize length fractionation. It is very easy to actually launch narrow (5 μm wide) bands of DNA in such structures using gold wires and electrostatic hold-down. However, at such small length scales diffusion begins to become very important (Tables 4–6).

Surface tension can be a powerful force at the micrometer scale. The equivalent pressure due to surface tension is given by the Laplace law,

$$P = \frac{2\gamma \cos\theta}{r}, \quad (22)$$

where θ is the contact angle between the liquid and the surface and r is the radius of curvature of the interface. This is the pressure one needs to overcome the surface tension. For instance, if a device is treated to be hydrophilic, water will naturally fill the channel, but stop at the exit. A pressure of at least $2\gamma \cos\theta/r$ (where r is the radius of the channel) will be needed to break through the surface tension and provide continuous flow. The contact angle between water and the silicon depends on the specific surface treatment, but if $\cos\theta = 1$, a hydrophilic surface, the equivalent pressure generated in a 3-μm diameter tube is about one atmosphere, a handy number to remember. Table 3 summarizes the pressure one must overcome due to surface tension. (Note that if the surface is hydrophobic, then this is the pressure one needs to just begin to force water into the channel.)

The surface energy can be used to drive liquid through the device. By treating the surface to be hydrophilic, water will penetrate through any size gap without any applied pressure. This penetration is driven by the attractive energy between the water and the surface. Fluid systems can be driven by this force. Plants, for instance, have a large evaporating surface (the leaf) and as water evaporates from the surface, more water is drawn up through the plant. Air bubbles pose a big problem in microfluid systems because of the small radius of curvature and hence large pressure required to overcome them. Air bubbles can form through two different ways. In the initial wetting of a hydrophilic device, air can become trapped where a wide channel necks

TABLE 2 Diffusion time in water at room temperature

Distance	Heat	Small Molecule	Protein	Cell
1 μm	10^{-4} s	10^{-1} s	10^{-2} s	10^1 s
10 μm	10^{-2} s	10^{-1} s	10^{0} s	10^3 s
100 μm	10^{0} s	10^{1} s	10^2 s	10^5 s
1000 μm	10^2 s	10^3 s	10^4 s	10^7 s

TABLE 3 Pressure due to surface tension inside a tube, for water

Radius & Pressure (dynes/cm²)	
0.15 μm	10^7
1.5 μm	10^6 (1 atmosphere)
15 μm	10^4
150 μm	10^3
1500 μm	10^2

TABLE 4 Water contact angle on surfaces treated in various ways

Surface Treatment	Contact Angle
SiO_2-untreated	43°
RCA-treated SiO_2	5°
Si-untreated	70°
Silanated SiO_2	95°

TABLE 6 Dimensionless fluid resistance for different geometries. The 2D sparse rectangles geometry is the one used in this paper. To calculate the required pressure drop for a certain fluid velocity, $\bar{u}$, multiply the dimensionless fluid resistance by $\bar{u}\eta/l^2$.

Geometry	Dimensionless Fluid Resistance
2D dense random packed spheres (He et al., 1992)	500
2D sparse rectangles (blood cell)	25
Pouiselle (circular tube)	$2\pi^2 \approx 19.7$
Hele-Shaw (two-dimensional sheet flow)	12

down to a smaller one (Lanzillotto et al., 1995). This is caused by the thin wetting layer jumping across the small opening before the air passes through. Air bubbles can also form after the device is wet, if air spontaneously comes out of solution. This often occurs when a cold solution warms up inside a device, lowering the solubility of gases dissolved in the liquid.

Water has one of the highest surface tensions of any common liquid, about three times higher than most others. Given this, a strategy to reduce air bubbles upon wetting is to wet the channel initially with a liquid that has a lower surface tension (such as isopropyl alcohol). Then water can be fed in behind the other liquid without exposing any air/water interface. This reduces by a factor of three the force due to surface tension that must be overcome to push air bubbles through a constriction. See Tables 4-6 for a summary of these results.

EXPERIMENTAL RESULTS

Some of the basic features of the above discussion are easily shown by observation of particles moving in microfabricated structures. Perhaps the most important aspect to flow at low Reynolds numbers is the profile of the velocity across the cross section of a channel, as a dispersion in velocity results in a dilution of the material being transported.

Verification of the predictions of Eq. 15 can be dramatically seen in Fig. 7. To obtain this result, 0.9-μm diameter fluorescent beads were passed along a channel etched into silicon of depth 11- and 72-μm width. The average bead velocity in the channel was approximately 20 μm/s. A trick was used to quickly get all the velocities of the beads: the electronic shutter of the CCD camera was set at 1/30th of a second so that the images of the beads consisted of elliptical streaks—the major axis of the ellipse is proportional to the bead speed. Approximately 100 beads/frame could be seen, and 10 frames were grabbed to get 1000 bead velocities. The software package NIH Image was used to create a table of ellipsoid ratios and the software package Kleidograph was used to produce an initial scatter plot of the measured velocities versus bead position in the channel. Because of
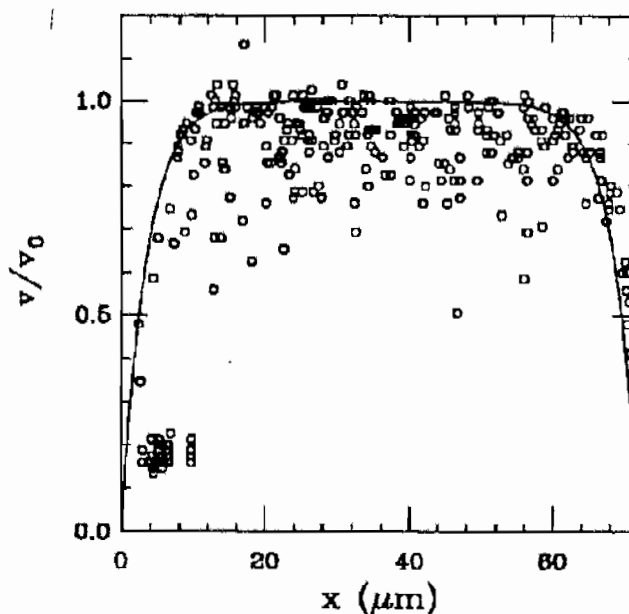
the relative thinness of the channel depth h, we did not attempt to ascertain the depth of each bead in the channel. Because of this, there is a scatter in the bead velocities due to the parabolic profile velocity along the thin h direction. The prediction of Eq. 15 is shown in Fig. 7 as a solid line. The excellent agreement between the predicted and measured values shows both how well you can understand flow at low Re and the interesting dispersion in fluid velocity in such high-aspect ratio rectangular channels.

Darcy's law can also be easily tested with microlithography. To do this experiment we used the variable-width blood cell array used in Brody et al., 1995. The rectangular blocks of dimension 4×13 μm were etched into silicon. Devices were fabricated with 2.5-, 3.0-, 3.5-, and 4.0-μm spacings between the rectangular blocks, and the fluid resistance was measured for these different structures. The measured flows through these devices was determined by tracking fluorescent beads through the structures as de

TABLE 5 Fluid properties at 20°C

	Density	Viscosity	Surface Tension	Vapor Pressure
Water	1.0 g/cm³	1.0 cP	72 dynes/cm	32.4 mm Hg
Isopropyl alcohol	0.8 g/cm³	2.5 cP	21 dynes/cm	17.5 mm Hg

FIGURE 7 Data on flow velocities in a channel. Beads velocities were measured as describe in the text and a scatterplot of velocities versus transverse position (x) in a 11-μm deep by 72-μm wide channel are plotted. The theoretical y-averaged velocity expected for an $\epsilon = 11/72$ is shown by the solid line.

scribed above and measuring the average velocities. The linearity between pressure head and average velocity shown in Fig. 8 confirms Darcy's Law.

The diffusion constant of objects at the micron scale, as we have mentioned, is important. In Fig. 9 a line of λ phage DNA 5 μm long is launched approximately 30 μm into a lattice of posts, which are 1 μm in diameter and 2 μm center-to-center spaced. The driving electric field is then removed and the approximately Gaussian distribution of molecules is tracked in time. In this case we once again work with λ phage DNA molecules that have been fluorescently labeled. The center of mass diffusion constant D_g of a flexible polymer is a very important quantity for many applications of biotechnology, and also is of interest because the same hydrodynamic considerations that modify the fluid flow profiles from the expected simple parabola also give an unexpected mass dependence to the diffusion constant of a polymer. In the absence of internal hydrodynamic coupling the diffusion constant of a polymer consisting of N links of effective radius b should simply scale with N. However, hydrodynamic coupling of the links as expressed by the Oseen-Burgers tensor approximation (Doi and Edwards, 1989) gives rise to a much weaker dependence of the translational diffusion constant with link number. Although the expression varies to some extent with the goodness of the solvent, to a reasonable approximation the diffusion constant is:

$$D_g \sim \frac{8k_B T}{3(6\pi^3)^{1/2}\eta b N^{1/2}} \qquad (23)$$

where b is twice the persistence length of the polymer. For double-stranded DNA $b \sim 300$ bp ~ 0.1 μm (Hogan and Austin, 1987). Thus, for λ phage DNA of size 47 kb $N \sim 150$ and $D_g \sim 4 \times 10^{-9}$ cm^2/s. We would then predict that in the elapsed time of 100 s shown in Fig. 9 that the FWHM of the initial 5-μm wide band should be approximately 20
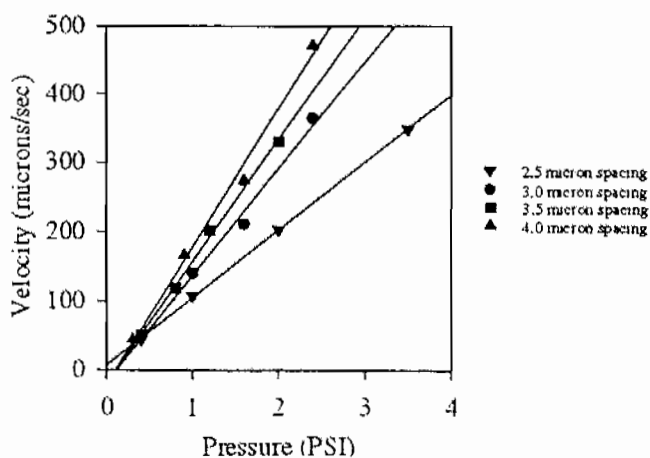

FIGURE 8   Darcy's Law measured in four different geometries. Each geometry had identical blocks, but different spacing. The permeability, k, is a function of the spacing, and in this figure is equal to the slope of the line.

μm, which it is. The lesson here is that even large molecules like λ phage DNA diffuse rapidly enough in micrometer-sized structures that fluid flow rates must be kept sufficiently high to prevent dilution of the material.

Fig. 10 illustrates the flow pattern through a complex structure with many dead ends. Lambda phage DNA molecules of total length about 20 μm were used as test "particles." However, because the DNA molecule has a very short persistence length, ($\approx$60 nm), the DNA forms a Gaussian coil with a radius of gyration R_g of approximately 1 μm. These curious particles are used here both to show the flow of biological molecules in these structures and because the Gaussian coil is sensitive to shear fields, which can unravel the Gaussian coil into a long continuous string. The polymer acts as a probe of highly shearing fields (Volkmuth, 1994). To visualize them, the DNA molecules are stained with ethidium bromide, a fluorescent dye, and imaged with epi-fluorescence microscopy. The velocity vectors of the flow pattern in the structure are evident as lines, and the intensity of the lines is a measure of the speed of the local flow. Rapidly moving particles leave a faint trace while slowly moving particles leave a bright trace. The increased velocity of the particles in the center of the channels is evident, and the slowly moving particles near the walls are also clear. Note also how the diffusion constant of the DNA molecules is small enough and the average velocity flow speed of approximately 10 μm/s is large enough that no penetration of the molecules into the numerous dead ends of the lattice are seen.

EXAMPLES OF DEVICES

Once the principles that govern fluid flow at the microscale are understood, they can be applied to construct useful devices. This section gives three examples of devices that have been constructed with these principles in mind.

We first consider how to make valves with no moving parts. Any complicated network of channels will require some means of switching between them. In macroscopic plumbing, this is accomplished by activating valves. In microscopic fluidic systems, this can be done by controlling the pressures to affect the flow streams—just as the voltages control the current in a network of resistors. We define the characteristic time, τ, as given by the condition that the first term of Eq. 2 is equal to unity. Pressure jumps over time scales longer than τ,

$$\tau = \frac{\rho l^2}{\eta}, \qquad (24)$$

can be considered quasi-static.

For water ($\rho = 1$ g/cm^3, $\eta = 10^{-2}$ P), in a channel 10 μm wide the characteristic time, τ, is equal to 100 μs. This allows one to use pressure controls to rapidly stop or change the direction of a liquid inside a microfluidic system while still retaining the simplifying assumptions of steady flow. The device shown in Fig. 11 is an intersection of four

5 microns

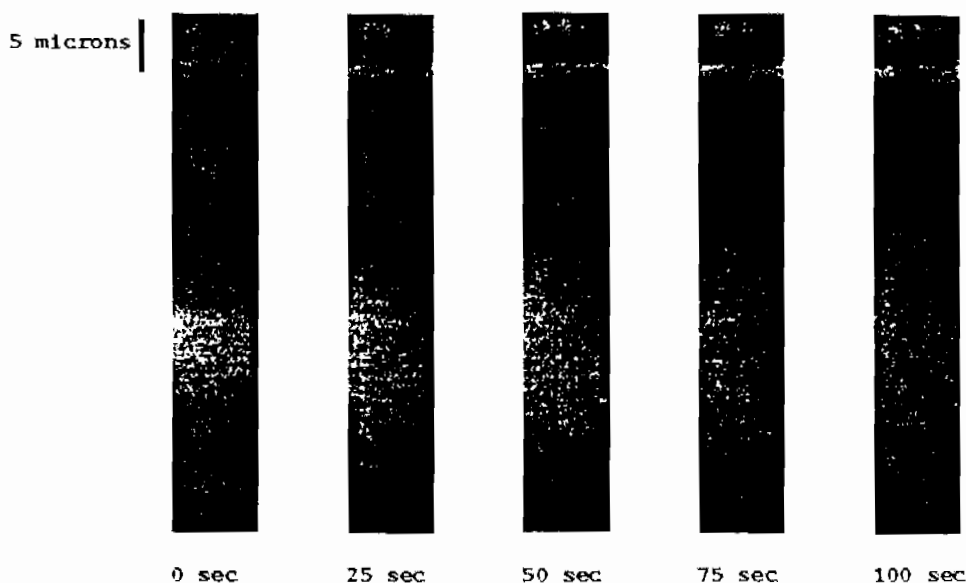0 sec   25 sec   50 sec   75 sec   100 sec

FIGURE 9 Self-diffusion of a launched DNA band. Ethidium bromide was used to stain a sample of λ phage DNA molecules of length 47 kbp. The DNA molecules were held by electrostatic fields against a gold wire and then launched from the wire into the array. After traveling approximately 30 μm the electric field was removed and the band was monitored versus time. The frames shown are 10 s apart.

channels. By controlling the pressure behind each of the four channels the flow can be directed from one channel to another, demonstrating a near zero dead volume valve. Fig. 11 demonstrates that the switching can take place on millisecond time scales.

Next, we consider how particles can be extracted from a flow by using diffusion. Extraction is a common laboratory process. Conventionally, it can be done in a number of

FIGURE 10 Ethidium bromide stained λ phage molecules moving by hydrodynamic flow in a percolating lattice. The DNA is imaged by epi-fluorescence. The average fluid velocity is approximately 10 μm/s, and the image was integrated for 20 s.

ways, for example by sedimentation or filtration. In a microfluidic system it can be done by diffusion-based extraction.

Diffusion can be used for extraction in a microfluid system—one in which the dimensions of the channels are sufficiently small that only low-Reynolds-number ($Re \ll 1$) flow can occur. Initially two separate flow streams (a carrier stream and a dilutant stream) are brought together into a central channel in which particles can diffuse between the two nonmixing streams. At higher Reynolds numbers ($Re \gg 10$), mixing independent of diffusion would occur between the two fluids in the central channel, but when the channels are small enough in size, the two adjacent streams flow in parallel without turbulence for the length of the channel. Only diffusive mixing will occur—even in low-viscosity fluids. At the end of the parallel flow channel a fraction of the carrier flow stream is split off into an output channel. The time for diffusive exchange between the two fluids, $t = l/v$, is controlled by the velocity, v, of fluid in the central channel and the length, l, of the channel.

A typical image allowing one to monitor the flow in such a device is shown in Fig. 12. A mixture of particles suspended in a carrier fluid enters a central channel from the bottom left and a diluting fluid enters from the top left. The ratio of carrier fluid to diluting fluid in the central channel is controlled by the pressure behind each of the two entrance channels. At the exit of the central channel, the fluid is split into two separate flow streams. Since the flow is in the low-Reynolds-number regime, this splitting can be done without any gross mixing. In this example, we extract fluorescent dye from a mixture of 0.5-μm beads and fluorescent dye.

Finally, we consider how to enhance mixing by an appropriately designed microfluidic device. An important example of the changes in device physics as dimensions shrink is the mixing chamber used in rapid reaction monitoring
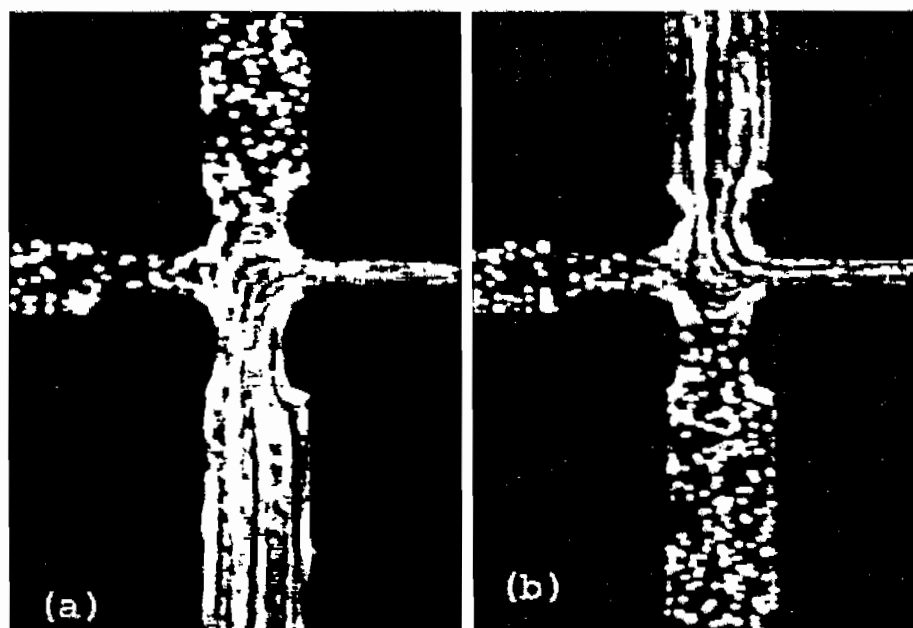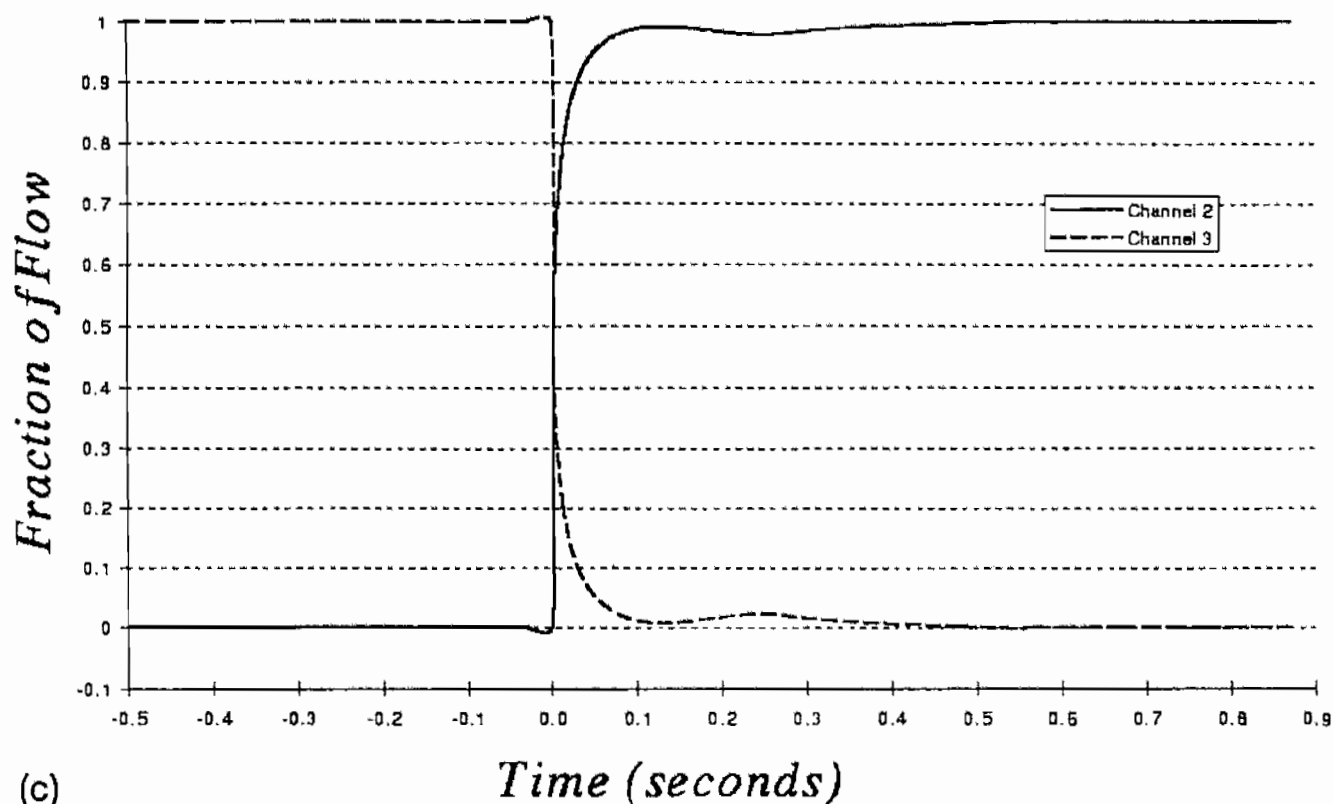
FIGURE 11   A virtual valve in a microfabricated fluidic system. This "valve" directs the flow at the intersection of the four channels. In this fluorescent image, 0.5-μm beads are used as flow tracers. The horizontal channel on the right is 10 μm wide. The flow is from right to left in the horizontal channel and then down (*a*) or up (*b*) the vertical channel. Note that the beads appear as streaks where the flow is occurring and as points where they are stationary. The direction of flow is controlled by the pressures behind each channel. The pressure behind the stopped channel are held at the pressure at the intersection of the channels. Because there is no pressure drop, there is no flow. In this case, the average flow velocity was about 100 μm/s, achieved with a pressure drop of about 1 psi. (*c*) The measured response time of the valve. Videotape was analyzed frame-by-frame to measure the fraction of flow.
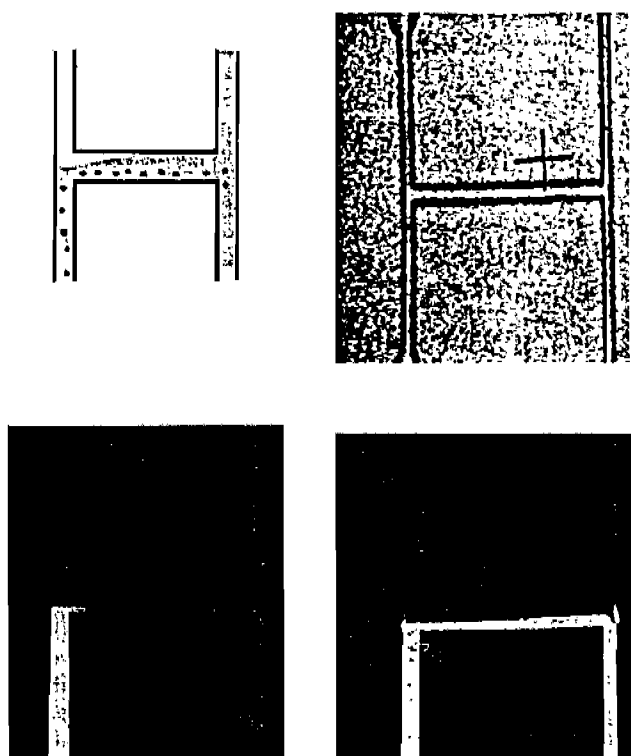
FIGURE 12 (a) A schematic diagram of a low Reynolds number "filter." Because of the unique properties of low Reynolds number flow (no mixing, laminar flow) a microfabricated fluidic filter can work like this. Two flow streams are brought into contact, one containing the sample and the other a dilutant (a buffer, for example). The flow streams move along a central channel where diffusion can occur between the two. At the end of the channel, the stream re-splits into two more streams, a waste stream and an output stream. Particles small enough to diffuse across the central channel will be found in the filter output, while larger (cell-sized) particles will not. (b) An optical image of the device used. The cross-hair is 100 μm × 100 μm. (c) A green fluorescent image of fluorescein flowing through the structure shown in (b). Fluorescein ($D \approx 500$ μm^2/s) was added to a 0.01% mixture of 0.2 μm red fluorescing balls ($D \approx 1$ μm^2/s). This green image shows the fluorescein flowing and diffusing across the central channel. The average velocity in the central channel was about 200 μm/s. Note that the output of this device the fluorescein is diluted by about a factor of two. (d) A red fluorescent image from the same experiment. The red fluorescence shows the slowly diffusing 0.2 μm balls. In this case they do not diffuse across the central channel and virtually all end up in the waste stream. The balls are too small and concentrated to be individually seen.

devices such as the stopped-flow apparatus. These devices rely on high Reynolds numbers to create turbulence, which can act as an efficient mixer of two streams of fluid. It would seem natural to shrink these devices beyond the typical millimeter length scale achievable by standard machining techniques. However, as the length of the mixing chamber shrinks and the Reynolds number decreases, one can pass from a region where turbulence provides effective mixing to one where turbulence ceases, the flow becomes laminar, and diffusion over possibly 10–100 μm becomes the primary mixing method. Unfortunately, diffusion can be a very slow process, and paradoxically, mixing times can *increase* with decreasing length scale unless basic changes

in the device design are made. Many microfluidic devices are near or at the regime where their design physics is limited by the decreasing Reynolds number—they can not be further scaled down without a basic change in the design. Comprehensive reviews of these devices have recently appeared (Gravesen et al., 1993; Northrup et al., 1995).

In a mixing chip design the essential feature is for two flows to come together and flow in close juxtaposition at high speed in a channel of decreased radius from the sum of the initial channels. When a fluid enters a narrow cylindrical channel from a wider one the flow profile is not immediately parabolic (Batchelor, 1967). After some distance l_d from the entrance of the channel, the flow is parabolic and the flow is referred to as fully developed. The distance, l_d, for flow to become 99% fully developed is only a function of the channel diameter, d, and the Reynolds number, Re (Duncan et al., 1970)

$$l_d \approx (0.5 + 0.065Re)d. \tag{25}$$

For low-Reynolds-number flow this distance is effectively $d/2$, so that this type of flow is almost immediately fully developed.

The idea behind this device is to have a large molecule (for instance, a protein) in the central channel and the smaller molecules with which it will be mixed in the side channels. Liquid from the central channel is squeezed down to a submicron wide lamina using hydrodynamic focusing (Sobek et al., 1994). Figure 13 presents some data from a micromachined device using four-port flow. The stream of protein should be completely mixed with the outer fluid in approximately $t = l^2/D$ where l is width of the lamina and D is the diffusion coefficient of the mixing species. For example, pH ($D = 10^4$ μm^2/s) jumps can be made in about 10 μs with a 0.1-μm wide lamina. As we show in the figure, by appropriate choosing of side jet and center jet pressures, focused streams of diameter ~0.1 μm can be achieved.

CONCLUSIONS

The physical effects that dominate in microfluid devices have been explored. It is perfectly feasible to construct and operate microfluid systems with dimensions as small as current technology allows (about 1 μm), although these devices behave in a manner quite different from experience at macroscopic scales. The fluid dynamics in microdevices is under low-Reynolds-number conditions, where turbulence and inertial effects are nonexistent. Mixing must be chiefly done by diffusion, and in fact diffusion cannot be neglected in the design of these devices. Forces due to surface tension at liquid/air interfaces are much stronger at this scale. Because the magnitude of these physical effects are different from what occurs at macroscopic scale, fluid-integrated microdevices must be designed from first principles, and not simply by miniaturizing macroscopic devices.
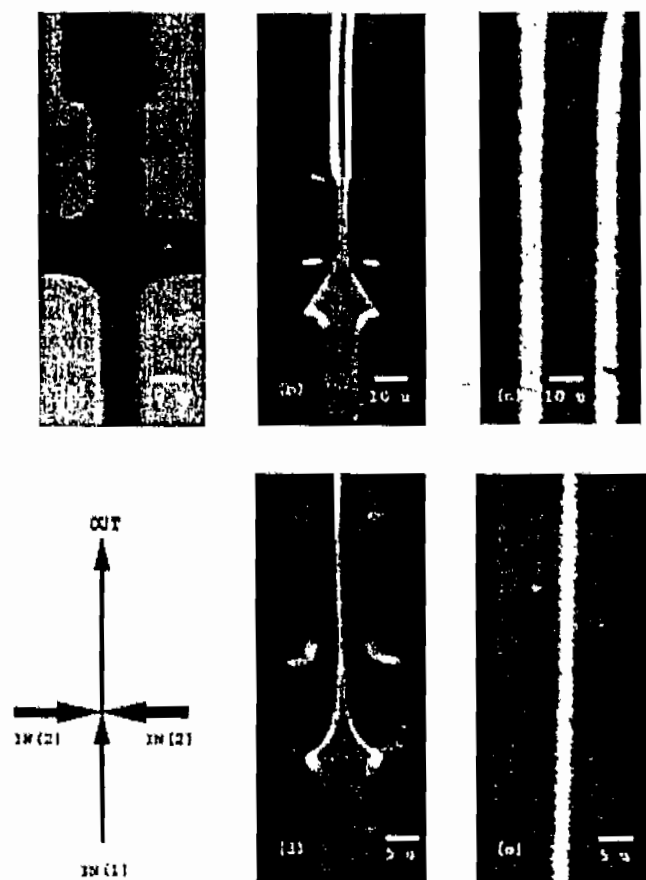
FIGURE 13 Hydrodynamic focusing in a four-channel port. (a) Config-uration of the completed device. Fluorescein in pH 3.0 buffer, 1 mM was injected from below at approximately 20 psi. pH 9.0 1 M buffer was injected from the two sides and the combination of the three streams was exited up the top channel. (b) When the side channel pressure is approx-imately equal to the center channel pressure little focusing occurs. This is an epi-fluorescence view of the dye stream. Note that diffusion of the pH 9 buffer into the pH 3 buffer stream results in enhancement of the fluorescein buffer in a sheath governed by the diffusion of the buffer components. (c) The low-focusing sheath viewed downstream from the original 10-μm wide sheath. The channel has widened to 100 μm width. (d) A highly focused beam. The side jet pressure is approximately twice the center jet pressure. (d) The highly focused jet seen downstream in a 100 μm widened stream. Extrapolation of the jet stream back to the original jet implies an initial width of ~0.1 μm.

discussions. Acquisition and analysis of the rectangular flow velocity and hydrodynamic focusing profiles was done by Amulya Vamsi Madhav at Princeton. Microfabrication work was done both at the Washington Tech-nology Center and the Cornell Nanofabrication Facility.

REFERENCES

Batchelor, G. K. 1967. An Introduction to Fluid Dynamics. Cambridge University Press, Cambridge, UK.

Bensimon, D., L. Kadanoff, S. Liang, B. I. Shraiman, and C. Tang. 1986. Viscous flows in two dimensions. Reviews of Modern Physics. 58: 977–999.

Bocquet, L., and J.-L. Barrat. 1993. Hydrodynamic boundary conditions and correlation functions of confined fluids. Phys. Rev. Lett. 70: 2726–2729.

Brody, J. P., Y. Han, R. H. Austin, and M. Bitensky. 1995. Deformation and flow of red blood cells in a synthetic lattice: evidence for an active cytoskeleton. Biophys. J. 68:2224–2232.

Brody, J. P., and P. Yager. 1996. Low reynolds number micro-fluidic devices. Solid State Sensor and Actuator Workshop, Hilton Head, South Carolina. 105–108.

Doi, M., and S. F. Edwards. 1989. The Theory of Polymer Dynamics. Oxford University Press, Oxford, UK.

Duncan, W. J., A. S. Thom, and A. D. Young. 1970. Mechanics of Fluids. Elsevier.

Gravesen, P., J. Branebjerg, and O. S. Jensen. 1993. Microfluidics—a review. Journal of Micromechanics and Microengineering. 3:168–182.

He, S., G. Kahandra, and P. Wong. 1992. Roughness of wetting fluid invasion fronts in porous media. Phys. Rev. Lett. 69:3731–3734.

Hogan, M. E., and R. H. Austin. 1987. The importance of DNA stiffness in protein-DNA binding specificity. Nature. 329:263–267.

Lanzillotto, A.-M., M. Amabile, T.-S. Leu, M. Sawicki, R. Wildes, and J. Dunsmuir. 1995. Real-time, 3D micro-imaging, visualization and anal-ysis of fluid transport in microelectromechanical systems. Eighth Inter-national Conference on Solid State Sensors and Actuators. 61–62.

Manz, A., D. J. Harrison, E. Verpoote, and H. M. Widmer. 1993. Planar chips technology for miniaturization of separation systems: a developing perspective in chemical monitoring. Adv. in Chromatogr. 33:1.

Northrup, M. A., G. Kovacs, P. Krulevitch, and A. P. Lee. 1995. MEMS for Medical and Biotechnological Applications. Unpublished Course Notes.

Peterson, K. E. 1982. Silicon as a mechanical material. Proc. IEEE. 70:420–457.

Purcell, E. M. 1977. Life at low reynolds number. Am. J. Physics. 45:3–11.

Ramsey, J. M., S. C. Jacobson, and M. R. Knapp. 1995. Microfabricated chemical measurement systems. Nat. Med. 1:1093–1096.

Sobek, D., S. Senturia, and M. L. Gray. 1994. Microfabricated fused silica flows chambers for flow cytometry. Solid State Sensors and Activators Workshop. Transducer Research Foundations.

Taylor, G. T. 1953. Dispersion of soluable matter in solvent flowing slowly through a tube. Proc. Roy. Soc. A. 225:186–203.

Volkmuth, W. 1994. Electrophoresis of Polyelectrolytes in Microfabri-cated Structures. Ph.D. thesis. Princeton University.

Volkmuth, W. D., and R. H. Austin. 1992. DNA Electrophoresis in a Microfabricated Structure. Nature. 358:600–602.

Wallis, G., and D. I. Pomerantz. 1969. Field Assisted Glass-Metal Sealing. J. Appl. Physics. 40:3946–3949.

Wilding, P., M. A. Shoffner, and L. J. Kricka. 1994. PCR in a Silicon Microstructure. Clin. Chem. 40:1815–1818.